Contrib Mineral Petrol (2007) 154:279–289
DOI 10.1007/s00410-007-0193-9

ORIGINAL PAPER

Influence of hydrogen on Fe–Mg interdiffusion in (Mg,Fe)O and implications for Earth's lower mantle

Sylvie Demouchy · Stephen J. Mackwell · David L. Kohlstedt

Received: 28 September 2006 / Accepted: 27 February 2007 / Published online: 15 March 2007

Abstract Interdiffusion of Fe and Mg in (Mg,Fe)O has been investigated experimentally under hydrous conditions. Single crystals of MgO in contact with $(Mg_{0.73}Fe_{0.27})O$ were annealed hydrothermally at 300 MPa between 1,000 and 1,250°C and using a Ni–NiO buffer. After electron microprobe analyses, the dependence of the interdiffusivity on Fe concentration was determined using a Boltzmann–Matano analysis. For a water fugacity of ~300 MPa, the Fe–Mg interdiffusion coefficient in $Fe_xMg_{1-x}O$ with $0.01 \leq x \leq 0.25$ can be described by $\tilde{D} = \tilde{D}_0 x^B \exp^{-(Q+Cx)/RT}$ with $\tilde{D}_0 = (5 \pm 1) \times 10^{-4}\,m^2\,s^{-1}$, $Q = 270 \pm 20\,kJ\,mol^{-1}$, $B = 0.8 \pm 0.1$, and $C = -80 \pm 10\,kJ\,mol^{-1}$. For $x = 0.1$ and at 1,000°C, Fe–Mg interdiffusion is a factor of ~4 faster under hydrous than under anhydrous conditions. This enhanced rate of interdiffusion is attributed to an increased concentration of metal vacancies resulting from the incorporation of hydrogen. Such water-induced enhancement of kinetics may have important implications for the rheological properties of the lower mantle.

Keywords Periclase · Fe–Mg interdiffusion · Hydrogen · Earth's mantle

Communicated by T.L. Grove.

S. Demouchy · S. J. Mackwell
Lunar and Planetary Institute, 3600 Bay Area Blvd, Houston, TX 77058, USA

S. Demouchy (✉) · D. L. Kohlstedt
Department of Geology and Geophysics, University of Minnesota, 310 Pillsbury Drive SE, Minneapolis, MN 55455, USA
e-mail: demou005@umn.edu

Introduction

Periclase[1] and perovskite are the principal minerals of the lower mantle. Perovskite is the most abundant mineral (~80% by volume), followed by periclase (~15% by volume) with a composition of $Mg_{1-x}Fe_xO$ with x between 0.1 and 0.2 (Ito and Takahashi 1987; Ringwood 1991; Guyot et al. 1988; Fiquet et al. 1998). Although periclase is unlikely to form an interconnected phase in the lower mantle, it is still one of the most abundant minerals inside the Earth, and its physical and chemical properties are of major interest for understanding the dynamics of the deep Earth (e.g., convection, chemical homogenization, rheological properties).

Previous studies on Fe–Mg interdiffusion in periclase (and iron-containing periclase) examined the effects of temperature, pressure and oxygen fugacity (Yamazaki and Irifune 2003; Holzapfel et al. 2003; Mackwell et al. 2005). Under dry conditions, Fe–Mg interdiffusion rates increase with increasing iron content and increasing oxygen fugacity, but decrease with increasing pressure by ~2.5 orders of magnitude from one atmosphere to 23 GPa (Mackwell et al. 2005).

Nominally anhydrous minerals of Earth's mantle (olivine and its high pressure polymorphs, as well as pyroxenes and garnet) incorporate water as hydrogen in conjunction with intrinsic point defects in their structure (Kohlstedt et al. 1996; Kohlstedt and Mackwell 1998; Ingrin and Skogby 2000; Bolfan-Casanova 2005). The presence of hydrogen in nominally anhydrous silicate minerals, even at very low

[1] Strictly speaking, this mineral presents in the lower mantle should be call ferropericlase but it is not a term approved by the International Mineralogical Association yet. Also, the same mineral (Mg,Fe)O containing only a small amount of Fe, has been call magnesiowüstite for many years.

concentrations, significantly affects many physical properties (e.g., Chopra and Paterson 1984; Mackwell et al. 1985; Hirth and Kohlstedt 1996; Mei and Kohlstedt 2000; Jacobsen et al. 2004). Hydrogen has also been proposed to enhance electrical conductivity (Karato 1990; Bahr and Simpson 2002; Huang et al. 2005; Yoshino et al. 2006; Wang et al. 2006). Nevertheless, little is known about the mobility of hydrogen and related point defects in lower mantle minerals. Recently, partitioning experiments have shown that hydrogen preferentially partitions into periclase rather than into silicate perovskite (Bolfan-Casanova 2000). However, $Mg_{0.93}Fe_{0.07}O$ and MgO can incorporate only a limited amount of hydrogen, with up to ~90 H/10^6 Mg (~20 ppm H_2O by weight) at 25 GPa and 1,200°C (Bolfan-Casanova et al. 2002; Bolfan-Casanova 2005).

The presence of hydrogen (protons) in olivine (Fo_{90}) enhances Si and O self-diffusion (Chakraborty and Costa 2004) as well as Fe–Mg interdiffusion (Wang et al. 2004; Hier-Majumder et al. 2004). Following the same idea, the aim of this study is to quantify the effect of hydrogen on Fe–Mg interdiffusion in periclase. Implications for the rheological properties of the lower mantle are discussed.

Experimental method

Sample preparation and experimental assembly

Our synthetic periclase single crystal samples were prepared from crystals of MgO following the method described by Mackwell et al. (2005). Laboratory grade oxide powders of Fe_2O_3 and MgO were mixed and baked twice at 1,400°C for 20 h under a controlled f_{O_2} of ~10^{-2} Pa using a CO/CO_2 gas mixture. Subsequently, MgO single crystals, as $5 \times 10 \times 0.5$ mm^3 (111) plates, were surrounded by the oxide powders and annealed in a gas mixing furnace at 1,450°C for >200 h at an f_{O_2} of ~10^{-2} Pa, controlled using a CO/CO_2 gas mixture. Interdiffusion of iron and magnesium between the powders and crystal resulted in single crystals with a homogeneous composition of $Mg_{0.73}Fe_{0.27}O$ and MgO single crystals were cut to dimensions $2 \times 2 \times 0.4$ mm^3 or $1 \times 1 \times 0.4$ mm^3 for the diffusion couples. The samples were polished on diamond lapping films with grit sizes from 30 down to 0.3 μm and cleaned using high-grade acetone. A Ni capsule was used as the sample container in order to buffer the oxygen fugacity near Ni–NiO during the diffusion experiment (~$10^{-3.7}$ Pa at 300 MPa and 1,300°C). The Ni capsules had an inner diameter of 10 mm with a relatively thick wall of 1 mm in order to slow loss of hydrogen during the diffusion experiment.

Each capsule was half filled with a 4:1 mixture of MgO (pre-fired at 800°C for ~24 h) and $Mg(OH)_2$ (brucite). This powder was uni-axially cold-pressed into the Ni can at 200 MPa. On this compacted layer, a second layer of powder was added and a small square indentation was made. The diffusion couple was placed in the indentation and covered by additional MgO–$Mg(OH)_2$ powder. A cold-pressed pellet of MgO, prepared in advance, was pushed into the Ni can. Finally, the Ni can was closed with a fitted Ni lid and arc-welded shut. The sealed Ni cans were stored in a desiccator until loading into the pressure vessel. During the diffusion experiments, the brucite in the sample capsule dehydrated, releasing ~100 μl of water.

Interdiffusion experiments

Interdiffusion experiments were performed using a gas-medium pressure vessel (Paterson 1990) at a confining pressure of 300 MPa and temperatures between 1,000 and 1,250°C under water-saturated conditions. The Ni can was encapsulated along with zirconia and alumina spacers inside an iron jacket, as described by Mei and Kohlstedt (2000). The temperature was controlled and monitored using an R-type thermocouple ($Pt/Pt_{0.87}Rh_{0.13}$). Based on temperature calibrations of the furnace, the temperature varies by less than 3°C along the Ni can (18 mm length) over the duration of the experiment. The temperature was increased to run conditions at ~50°C min^{-1}. The sample was cooled to 300°C in 10–12 min, at which point diffusion had effectively ceased. After the experiment, each capsule was pierced to check for the presence of excess water (i.e., water and gas bubbling out from the capsule) to ensure that the system was water-saturated during the diffusion anneal.

Two experiments (PI-1270 and PI-1245) were performed at the same pressure, temperature and time (300 MPa, 1,250°C, 5 h) to test for reproducibility, and two other experiments (PI-1240 and PI-1265) were performed at the same temperature but for different durations (1,250°C, 2 and 10 h, respectively). Two additional experiments (PI-1292 and PI-1293) were performed under anhydrous (brucite-free) conditions for comparison with the hydrous experiments. Experiment PI-1293 was quenched one minute after reaching the diffusion temperature to test for any effects of heating up and cooling down on the diffusion profile.

Analytical methods

The recovered interdiffusion couples were cut in half perpendicular to the interface between the crystals using a diamond saw blade (0.14 mm thick). Half was mounted in Crystal Bond™, polished using diamond-lapping film down to 0.5 μm, and carbon coated for electron microprobe analysis. The other half of each diffusion couple was

doubly polished for Fourier transform infrared (FTIR) analysis.

Electron microprobe analyses

The chemical homogeneity of the starting material and the Fe–Mg concentration profiles were determined using a JEOL JXA-8200 electron microprobe (15 keV, 15 nA, point beam, 40 s counting time). The following elements were analyzed with the detection limits in ppm by weight given in brackets: Fe (156), Mg (77), Si (106), Al (81), Ni (200). The standards were forsterite (Mg), olivine (Fe, Si), Ni metal (Ni), and augite (Al). First, concentration profiles were obtained across the entire diffusion couple on a line perpendicular to the initial interface with a step distance of 10 μm. Because the two single crystals bonded, the initial interface was, in a few cases, hard to locate after the interdiffusion experiment; however, these 10-μm step profiles permitted location of the initial interface. Second, additional concentration profiles, obtained closer to the initial interface with a step distance of 2 μm, were used for determination of the diffusion coefficients. No difference in concentration was observed between the 10- and 2-μm step profiles.

Fourier-transform infrared analysis

Water concentrations within our samples were analyzed using unpolarized FTIR spectroscopy collected with a Bruker IFS 120 HR FTIR spectrometer coupled with an IR microscope at the Bayerisches Geoinstitut. The analytical set up, previously described by Demouchy and Mackwell (2003), used an aperture of 100 μm diameter; 400 scans were accumulated. The homogeneity of the hydroxyl distribution was analyzed using a FTIR spectrometer Nicolet Magna-IR 750 coupled with an IR microscope at the University of Minnesota, also using unpolarized infrared radiation. To check the homogeneity of the hydroxyl distribution, spectra were collected at a spacing of 50 μm perpendicular to the diffusion couple interface in the transparent MgO part of the diffusion couple, using a square aperture 120 × 120 μm^2; 200 scans were accumulated. The more Fe-rich part of the diffusion couple totally absorbed the IR radiation, so FTIR analyses were not possible on the (Mg,Fe)O part of the diffusion couple. The analyzed MgO part of each diffusion couple was in all cases clean and transparent (no turbid, cloudy, or milky areas). After background-baseline correction and thickness normalization to 1 cm, the hydroxyl content was determined for each spectrum using the calibration given by Paterson (1982). This calibration is commonly chosen in the absence of specific calibrations for a given mineral (Bolfan-Casanova 2000; Rauch and Keppler 2002). This calibration, which may underestimate the water content in some minerals (Libowitzky and Rossman 1996; Bell et al. 2003), is based on an empirical correlation between OH stretching frequency and extinction coefficient; it leads to the following expression:

$$C_{OH} = \frac{\varphi_i}{150\xi} \int \frac{k(v)}{3,780 - v}\, dv, \quad (1)$$

where C_{OH} is the concentration of hydroxyl, ξ is an orientation factor that equals 1/3 for unpolarized measurements, $k(v)$ is the absorption coefficient for a given wavenumber v, φ_i is the density factor, which is chemistry dependent: $\varphi_i = 1.125 \times 10^4$ H/10^6 O or 2,513 ppm H_2O by wt for MgO (Bolfan-Casanova 2000). Integration was performed from v = 3,200–3,500 cm^{-1}.

Point defects in (Mg,Fe)O

Under anhydrous conditions, the majority point defects in (Mg,Fe)O are V''_{Me} and $Fe^{\bullet}_{Me}$ (Valet et al. 1975; Gourdin and Kingery 1979) such that the charge neutrality condition is

$$[Fe^{\bullet}_{Me}] = 2[V''_{Me}], \quad (2)$$

where the subscript indicates the type of site occupied by the chemical species, the superscript indicates the charge relative to the given site ($^{\bullet}$ for a positive charge, $'$ for a negative charge, and $^{\times}$ for neutral), and V indicates a vacant site according to the Kröger–Vink notation (Kröger and Vink 1956); the square bracket indicates defect species concentration per molecule of mineral.

The formation of a metal vacancy to balance the ferric iron atoms in normal metal sites is written as

$$\frac{1}{2}O_2\,(g) + 2Fe^{\times}_{Me} + Me^{\times}_{Me} \leftrightarrows 2Fe^{\bullet}_{Me} + V''_{Me} + MeO\,(srg), \quad (3)$$

where g means ''in the gas phase'' and srg means ''a site of repeatable growth''. The law of mass action applied to the reaction in Eq. 3 yields

$$K_3[Fe^{\times}_{Me}]^2 f_{O_2}^{1/2} = [Fe^{\bullet}_{Me}]^2\,[V''_{Me}], \quad (4)$$

where K_3 is the equilibrium constant for the reaction in Eq. 3

a_{MeO}= 1, and $[Me^{\times}_{Me}] \approx 1$.

By combining Eqs. 2 and 4 we obtain

$$\frac{1}{2}[\mathrm{Fe}^{\bullet}_{\mathrm{Me}}] = [\mathrm{V}''_{\mathrm{Me}}] = \sqrt{[3]}K_3/4 f_{\mathrm{O}_2}^{1/6}[\mathrm{Fe}^{\times}_{\mathrm{Me}}]^{2/3}. \quad (5)$$

Under hydrous conditions, other charge neutrality conditions may apply, such as

$$[(\mathrm{OH})^{\bullet}_{\mathrm{O}}] = 2[\mathrm{V}''_{\mathrm{Me}}], \quad (6)$$

where $(\mathrm{OH})^{\bullet}_{\mathrm{O}}$ defects are essentially interstitial protons. The reaction that describes the incorporation of hydrogen into MeO via the formation of these two point defects is

$$\mathrm{H_2O\,(fl)} + \mathrm{Me}^{\times}_{\mathrm{Me}}, +2\mathrm{O}^{\times}_{\mathrm{O}} \leftrightarrows \mathrm{V}''_{\mathrm{Me}} + 2\,(\mathrm{OH})^{\bullet}_{\mathrm{O}} + \mathrm{MeO\,(srg)}, \quad (7)$$

where fl means ''in the fluid phase''. Applying the law of mass action to Eq. 7, we obtain

$$K_7 f_{\mathrm{H_2O}} = [\mathrm{V}''_{\mathrm{Me}}]\,[(\mathrm{OH})^{\bullet}_{\mathrm{O}}]^2. \quad (8)$$

By combining Eqs. 6 and 8, we obtain

$$\frac{1}{2}[(\mathrm{OH})^{\bullet}_{\mathrm{O}}] = [\mathrm{V}''_{\mathrm{Me}}] = \sqrt{[3]}K_7/4\ f_{\mathrm{H_2O}}^{1/3}. \quad (9)$$

In the case of the present experimental study, ferric iron and hydrogen are both present in the system. Therefore, another possible charge neutrality condition is

$$[\mathrm{Fe}^{\bullet}_{\mathrm{Me}}] = [\{(\mathrm{OH})^{\bullet}_{\mathrm{O}} - \mathrm{V}''_{\mathrm{Me}}\}'], \quad (10)$$

where $\{(\mathrm{OH})^{\bullet}_{\mathrm{O}} - \mathrm{V}''_{\mathrm{Me}}\}'$ are defect associates formed between a proton and a metal vacancy. For this charge neutrality condition, the concentration of $\{(\mathrm{OH})^{\bullet}_{\mathrm{O}} - \mathrm{V}''_{\mathrm{Me}}\}'$ defects must be twice the number of unassociated metal vacancies. The reaction describing the incorporation of hydrogen into (Mg,Fe)O via the majority point defects in Eq. 10 is

$$\frac{1}{2}\mathrm{O_2\,(g)} + \mathrm{H_2O\,(fl)} + 2\mathrm{Me}^{\times}_{\mathrm{Me}} + 2\mathrm{O}^{\times}_{\mathrm{O}} + 2\mathrm{Fe}^{\times}_{\mathrm{Me}} \leftrightarrows 2\mathrm{Fe}^{\bullet}_{\mathrm{Me}} + 2\{(\mathrm{OH})^{\bullet}_{\mathrm{O}} - \mathrm{V}''_{\mathrm{Me}}\}' + 2\mathrm{MeO\,(srg)}. \quad (11)$$

Applying the law of mass action to Eq. 11, we obtain

$$K_{11}\ f_{\mathrm{O}_2}^{1/2} f_{\mathrm{H_2O}}[\mathrm{Fe}^{\times}_{\mathrm{Me}}]^2 = [\mathrm{Fe}^{\bullet}_{\mathrm{Me}}]^2[\{(\mathrm{OH})^{\bullet}_{\mathrm{O}} - \mathrm{V}''_{\mathrm{Me}}\}']^2. \quad (12)$$

Combining Eq. 10 with Eq. 12 we find

$$[\{(\mathrm{OH})^{\bullet}_{\mathrm{O}} - \mathrm{V}''_{\mathrm{Me}}\}'] = [\mathrm{Fe}^{\bullet}_{\mathrm{Me}}] = \sqrt{[4]}K_{11}[\mathrm{Fe}^{\times}_{\mathrm{Me}}]^{1/2} f_{\mathrm{H_2O}}^{1/4} f_{\mathrm{O}_2}^{1/8}. \quad (13)$$

Equation (13) predicts a direct dependence of the hydroxyl concentration on iron content.

Previous studies on diffusion in periclase, Fe-bearing periclase and olivine have demonstrated that the total concentration of cation vacancies increases with increasing iron content (Gordon 1985; Zhao et al. 2004), such that

$$[\mathrm{V}''_{\mathrm{Me}}]^{\mathrm{tot}}_{(\mathrm{Fe,Mg})\mathrm{O}} > > [\mathrm{V}''_{\mathrm{Me}}]^{\mathrm{tot}}_{\mathrm{MgO}}, \quad (14)$$

where $[\mathrm{V}''_{\mathrm{Me}}]^{\mathrm{tot}}$ denotes here the total concentration of vacancies with or without the presence of hydrogen in the system.

The presence of hydrogen is expected to result in the formation of additional cation vacancies through reactions such as Eq. 11. Thus we can write

$$[\mathrm{V}''_{\mathrm{Me}}]^{\mathrm{tot}} = [\mathrm{V}''_{\mathrm{Me}}] + [\{(\mathrm{OH})^{\bullet}_{\mathrm{O}} - \mathrm{V}''_{\mathrm{Me}}\}'] + [\{2(\mathrm{OH})^{\bullet}_{\mathrm{O}} - \mathrm{V}''_{\mathrm{Me}}\}^{\times}]. \quad (15)$$

It is also possible that the charge neutrality condition may change with changes in iron and/or hydrogen concentration (and hence position) along the diffusion couples in our experiments.

Diffusion analysis

To determine the interdiffusion coefficients using the Boltzmann–Matano analysis, the concentration profile was first fit to the function (Holzapfel et al. 2003; Holzapfel 2004; Mackwell et al. 2005)

$$c(z) = A_0\left(1 - \frac{1}{(1+\exp(A_1 z + A_2))^{A_3}}\right), \quad (16)$$

where c the concentration, z is the distance (perpendicular to the initial interface), and A_0, A_1, A_2, and A_3 are fitting parameters. Second, the Matano interface was determined by integrating across the profile until the following equation is satisfied (Matano 1933)

$$\int_0^{c_{\mathrm{m}}} z\mathrm{d}c = 0, \quad (17)$$

where c_{m} is the maximum concentration. In the third step, the Boltzmann–Matano analysis was applied to the fitted concentration profile to obtain the concentration-dependent interdiffusion coefficient, $\tilde{D}(c^*)$:

$$\tilde{D}(c^*) = -\frac{1}{2t}\left(\frac{\mathrm{d}x}{\mathrm{d}c}\right)_{c^*}\int_0^{c^*} z\mathrm{d}c, \tag{18}$$

where t the duration of the diffusion experiment.

The derivative term in Eq. 18 was determined by differentiating Eq. 16, while the actual data are used to calculate the integral term, as described in Mackwell et al. (2005). In this way the entire data set was fit (a ''global fit'') by varying $\tilde{D}_0, Q, B$ and C in the following equation to define the interdiffusion coefficient (see Schmalzried 1981, p. 38; Mackwell et al. 2005):

$$\tilde{D} = \tilde{D}_0\, x^B\, \exp^{-(Q+Cx)/RT}\ \mathrm{m}^2\,\mathrm{s}^{-1}, \tag{19}$$

where $\tilde{D}_0$ is the pre-exponential term, which includes the oxygen fugacity and water fugacity dependences, $(Q + Cx)$ is the composition-dependent activation energy, B and C are fitting parameters, x is the mole fraction of FeO, T is the absolute temperature, and R is the gas constant. In this description, the activation energy was expanded in a Taylor series to describe its dependence on x. Only the first term of the expansion is required to fit the experimental data (Schmalzried 1981, p. 38 ; Zhao et al. 2004; Mackwell et al. 2005).

Assuming that the oxygen sublattice is immobile compared to the cations in $Fe_xMg_{1-x}O$ (i.e., the Matano interface is coincident with the original interface), the interdiffusion coefficient can be written as a function of the self-diffusivities (D_i) of the diffusing cations (i = Mg, Fe) according to the Nernst–Planck relation (Schmalzried 1981, p. 103):

$$\tilde{D}_{\mathrm{Fe-Mg}} = \frac{D_{\mathrm{Fe}}D_{\mathrm{Mg}}}{xD_{\mathrm{Fe}} + (x-1)\,D_{\mathrm{Mg}}}, \tag{20}$$

where x is the mole fraction of FeO. We assume that the thermodynamic factor is unity, as the (Mg,Fe)O solid solution is nearly ideal for the composition and conditions investigated in this study.

Since the cation self-diffusivities are related to the vacancy self-diffusivity and its concentration (Nakamura and Schmalzried 1984) through

$$D_i \approx D_{\mathrm{V}}\,[\mathrm{V}''_{\mathrm{Me}}]^{\mathrm{tot}}, \tag{21}$$

the interdiffusion coefficient for the present study is given by

$$\tilde{D}_{\mathrm{Fe-Mg}} = D_{\mathrm{V}}\,[\mathrm{V}''_{\mathrm{Me}}]^{\mathrm{tot}}. \tag{22}$$

Therefore, the dependence of $\tilde{D}_{\mathrm{Fe-Mg}}$ on x and $f_{\mathrm{H_2O}}$ enters through the dependence of the total vacancy concentration in the presence of hydrogen on these quantities.

Results

Fe–Mg interdiffusivity

The transmitted light micrograph in Fig. 1 shows the diffusion zone between MgO and (Mg,Fe)O, as well as the initial interface in sample PI-1238. The two crystals of the diffusion couple bonded, during the high-temperature diffusion anneals at temperatures over 1,100°C. The cracks did not modify the concentration profiles, indicating that they formed either during the quench or during the preparation of the sample for microprobe analyses.

An interdiffusion profile for a sample annealed for 2 h at 1,200°C as well as the fit to Eq. 16 is shown in Fig. 2. Although the interdiffusion profile is clearly asymmetric, it is fit well by this equation. Using this fitted curve in

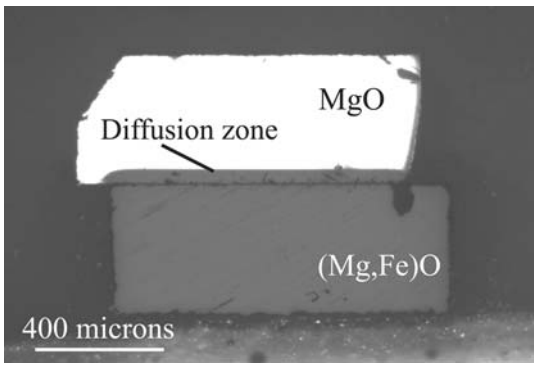

Fig. 1 Photomicrograph of a diffusion couple after a interdiffusion experiment (PI-1238) at 1,200°C

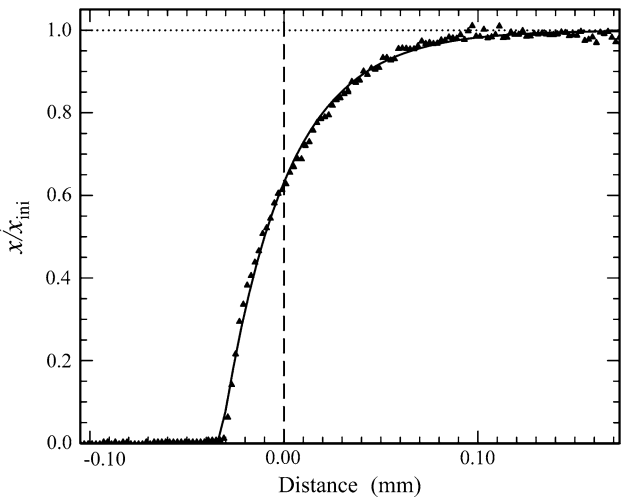

Fig. 2 Concentration profile (x = Fe/(Fe + Mg)) of a sample (PI-1240), annealed at 300 MPa, 1,250°C for 2 h, as a function of the position in the diffusion couple perpendicular to the original interface. Initial interface is set at $z = 0$. The *solid line* shows the non-linear least square fit to the data

combination with the Boltzmann–Matano analysis, we obtain the interdiffusion coefficients as a function of iron content. The resulting Fe–Mg interdiffusion coefficients for two compositions, $x = 0.1$ and $x = 0.2$, are summarized in Table 1.

Experiments PI-1240 and PI-1265 were performed at the same temperature, 1,250°C but for different durations, of 2 and 10 h. Within error, no significant difference was observed in the calculated diffusion coefficients, demonstrating that the interdiffusivity is independent of time.

The interdiffusion coefficients for each experiment in this study are plotted as a function of x in Fig. 3. The Fe–Mg interdiffusivities increase systematically with increasing temperature and increasing iron concentration. A global fit using Eq. 19 to all of the data in Fig. 3 yields $\tilde{D}$ as a function of iron concentration x and absolute temperature T:

$$\tilde{D} = (5 \pm 1 \times 10^{-4}) x^{(0.8 \pm 0.1)} \exp[-((270 \pm 20\,\mathrm{kJ\,mol^{-1}}) + (-80 \pm 10\,\mathrm{kJ\,mol^{-1}})x)/RT] \quad (23)$$

with $\tilde{D}$ in $\mathrm{m^2\ s^{-1}}$.

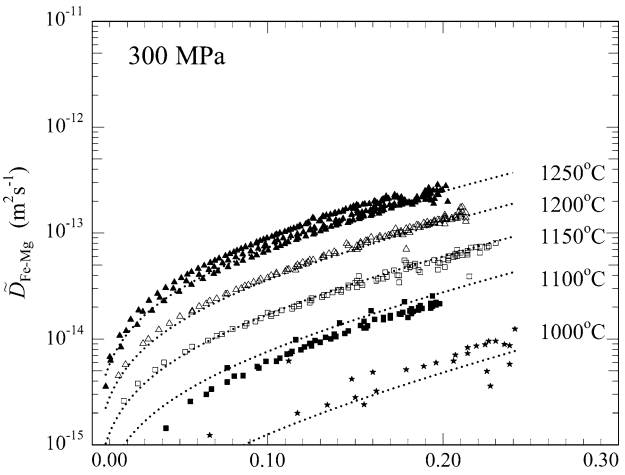

Fig. 3 Fe–Mg diffusion coefficients as a function of x obtained using the Boltzmann–Matano analyses for experiments at 300 MPa and for various temperatures, with the oxygen fugacity buffered along Ni–NiO. The *dotted lines* are the result of the global fit to the data (see text for details)

Infrared spectra and hydrogen concentrations

In the unpolarized infrared spectra from the MgO samples measured after the diffusion experiments, given in Fig. 4, two IR bands are distinguishable, one at 3,310 $\mathrm{cm^{-1}}$ and the other at 3,296 $\mathrm{cm^{-1}}$. Comparison with previous studies reveals that (1) our infrared spectra differ from those for undoped MgO hydrated at 25 GPa (Bolfan-Casanova 2000, 2005), (2) our infrared spectra are similar to Al-doped MgO hydrated at 25 GPa (Bolfan-Casanova 2005), and (3) the infrared spectra from this study are similar to cation-doped as well as undoped MgO crystals synthesized at room pressure and high temperature (Gonzalez et al. 1982). Electron microprobe analyses did not detect any other divalent or trivalent cations in concentrations higher

Table 1 Experimental conditions and resulting Fe–Mg interdiffusivities

Run no.	Temperature (°C)	Duration (h)	[c]f_{O_2} (Pa)	[d]f_{H_2O} (MPa)	Water content H/10^6 O (ppm H_2O wt)	log (D_{Fe-Mg})	
						$x = 0.1$	$x = 0.2$
PI-1230	1,090	12	10^{-4}	295	3 ± 1 (0.7 ± 0.2)	–14.2	–13.6
PI-1234	1,150	8	$10^{-3.2}$	320	11 ± 4 (2.7 ± 0.8)	–13.7	–13.3
PI-1238	1,200	5	$10^{-2.6}$	326	15 ± 4 (3.5 ± 1)	–13.4	–12.9
PI-1240	1,250	2	$10^{-2.1}$	330	NA	–13.3	–12.7
PI-1242	1,000	10	$10^{-5.2}$	295	2.2 ± 0.4 (0.5 ± 0.1)	–14.8	–14.2
PI-1245	1,250	5	$10^{-2.1}$	330	NA	–13.1	–12.6
PI-1265	1,250	10	$10^{-2.1}$	330	NA	–13.0	–12.5
PI-1270	1,250	5	$10^{-2.1}$	330	20 ± 6 (4.5 ± 1.3)	–13.1	–12.5
PI-1292[a]	1,230	2	$10^{-2.3}$	–	–	–13.6	–12.9
PI-1293[a,b]	1,250	0	–	–	–	–	–

The pressure was identical for all experiments at 300 ± 5 MPa

NA Not analyzed (due to difficulties in sample preparation for FTIR)

[a] Anhydrous conditions

[b] Heating step only, the diffusion profile was less than 10 μm long and diffusion analysis was not possible, demonstrating that diffusion during the heating step is not significant

[c] Calculated according to O'Neill and Wall (1987)

[d] Calculated according to Pitzer and Sterner (1994)

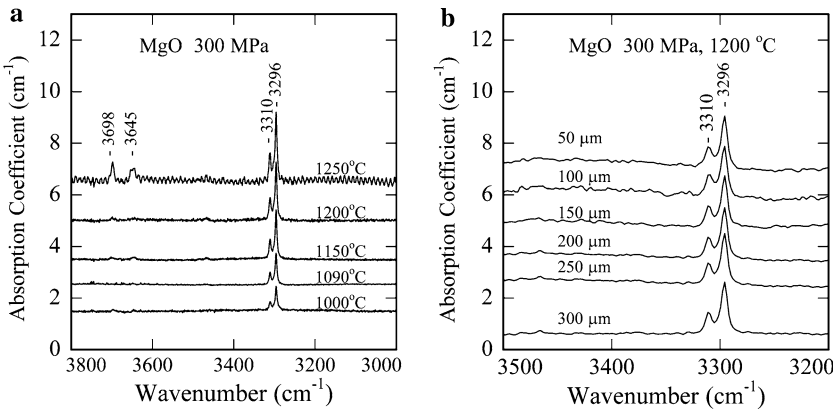

Fig. 4 **a** Series of unpolarized infrared spectra for various positions, along a profile perpendicular to the original interface, in the MgO part of the diffusion couple (PI-1238) after an experiment at 300 MPa and 1,200°C for 5 h buffered with Ni–NiO. **b** Unpolarized infrared spectra from the MgO region for diffusion couples annealed at several temperatures (PI-1230, PI-1234 PI-1238, PI-1240, PI-1242 and PI-1270)

than the detection limit (e.g., for aluminum: 352 Al/10^6Si ≈ 80 ppm Al by weight). As the hydrogen concentrations determined by the spectra are considerably below the electron microprobe detection limits for such cations, the role of any impurities, including Al, in defining the hydroxyl band positions is uncertain. A series of spectra (Fig. 4b), taken at 50 µm intervals and perpendicular to the diffusion interface in the MgO part of the diffusion couple after annealing at 1,200°C, reveals no variations in the intensity and area of the IR bands, indicating that the distribution of hydroxyl in the MgO part of the diffusion couple is homogeneous and that water-saturation has been reached.

A comparison of spectra obtained from samples annealed from 1,000 to 1,250°C in Fig. 4a indicates that the intensity and area of the IR bands increase with increasing temperature. The corresponding water concentration increases from 2.2 H/10^6 O (~0.5 ppm H_2O by weight) to ~20 H/10^6 O (~4.5 ppm H_2O by weight). The temperature dependence of the water solubility at a fluid pressure of 300 MPa in MgO can be then obtained by fitting the data (Table 1) with the following equation:

$$C_{OH} = A f_{H_2O}^{n} \exp\left(\frac{-H}{RT}\right), \quad (24)$$

where C_{OH} is the concentration in hydroxyl in H/10^6 O, A is a constant in (H/10^6 O)/MPa^n, f_{H_2O} is the water fugacity, which was calculated using the equation of state for H_2O reported by Pitzer and Sterner (1994), the value of the exponent n depends on the mechanism of incorporation for hydrogen in MgO, and H is the activation enthalpy for incorporation of OH in MgO. The linear fit shown in Fig. 5 yields H = 150 ± 20 kJ mol^{-1}. As the experiments were performed over a very narrow range of water fugacity (Table 1), it was not possible to calculate the fugacity exponent, n, independently. However, potential values for n are provided from the point defect relations, such as Eqs. 9 and 13, for particular charge neutrality conditions. If we use an exponent n equal to 1/3, as in Eq. 9, A = $10^{5.8\ \pm\ 0.5}$ H/10^6 O/MPa$^{0.33}$. If n = 1/2, as would be expected when no hydrogen defects participate in charge neutrality, then A = $10^{5.2\ \pm\ 0.5}$ H/10^6 O/MPa$^{0.5}$. It is also interesting to note that, if charge neutrality were defined by the charge neutrality condition $\{(OH)_O^{\bullet} - V''_{Me}\}' = [(OH)_O^{\bullet}]$, one would expect a solubility exponent of n = 1. This condition is likely to hold for end-member periclase under wet conditions where iron cannot participate in charge neutrality.

As also shown by Fig. 4a, for an experiment performed at 1,250°C, two additional minor bands are present, one at 3,698 and the other at 3,645 cm^{-1}. These infrared bands are attributed to the presence of brucite (Shinoda et al. 2002;

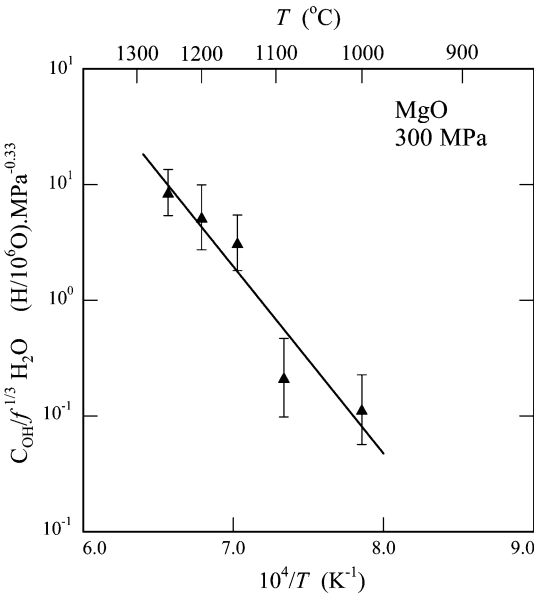

Fig. 5 Arrhenius diagram of $C_{OH}/f_{H_2O}^{1/3}$ as a function of the inverse absolute temperature. Only the IR bands at 3,310 and 3,296 cm^{-1} were taken in consideration for the calculation of the OH content in MgO. The *solid line* results from a linear least squares fit to the data set

Bolfan-Casanova et al. 2002). Therefore, these IR bands were not taken into account when integrating to obtain the water concentration.

Discussion

Influence of hydrogen on the interdiffusivity

From Eqs. 14 and 22, it is expected that the gradient in cation vacancy concentration associated with the gradient in Fe concentration should result in (1) lower values for $\tilde{D}_{\mathrm{Fe-Mg}}$ in the iron-depleted, vacancy-poor MgO part of the diffusion couple, which is consistent with the strong asymmetry of the concentration profiles (Fig. 2), and (2) an increase of $\tilde{D}_{\mathrm{Fe-Mg}}$ under hydrous conditions compared to $\tilde{D}_{\mathrm{Fe-Mg}}$ under anhydrous conditions. Since periclase is cubic (rock salt structure), ionic diffusion is isotropic, such that the Fe–Mg interdiffusion coefficients obtained here for the [111] direction are directly comparable to the interdiffusivities reported by Mackwell et al. (2005) for the [100] direction. As shown in Fig. 6, for any given value of x, the Fe–Mg interdiffusion coefficient under hydrous condition is ~4 times faster than under anhydrous conditions for an oxygen fugacity along Ni–NiO. Interdiffusion experiments under relatively low water fugacity conditions obtained using CO_2/H_2 gases in a 1-atm furnace, revealed no measurable effect of hydrogen (Mackwell et al. 2005). The difference between our interdiffusion measurements under hydrous conditions at a pressure of 300 MPa and their study at one atmosphere is attributed to the difference in water fugacity, ~300 MPa compared to 0.08 MPa. Based on the results reported here, we would expect to see no water enhancement of diffusion at such low water fugacities. Our interdiffusion coefficients determined under anhydrous conditions (PI-1292) are in good agreement with the results of the one-atmosphere experiments of Mackwell et al. (2005).

Although these experiments sampled only limited ranges of water fugacity, oxygen fugacity and temperature, it is possible to compare the interdiffusion coefficient given in Eq. 23 with theoretical models based on point defect thermodynamics (e.g., Eqs. 3–15) in order to gain greater insight into the way in which hydrogen interacts with the (Mg,Fe)O, enhancing the rate of diffusion. As noted above, the experiments demonstrate a power law dependence for $x \approx [\mathrm{Fe}^{\times}_{\mathrm{Me}}]$ (Eq. 19) with exponent $B \approx 0.8$, a positive dependence on water fugacity, and $Q = 270$ kJ mol^{-1}. As the oxygen fugacity was buffered in all cases by Ni–NiO, a dependence on oxygen fugacity could not be determined; however, the measured activation energy may include some component due to the temperature dependence of oxygen fugacity for this buffer.

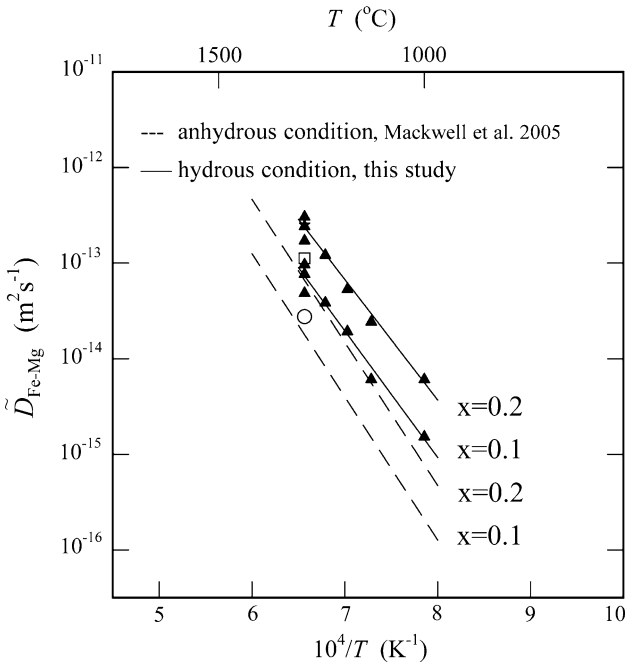

Fig. 6 Fe–Mg interdiffusion coefficients in (Mg,Fe)O under hydrous conditions with the experiments buffered at Ni–NiO for two different chemical compositions $x = 0.1$ and $x = 0.2$. For comparison, Fe–Mg interdiffusion coefficients under dry conditions from this study (*open square* and *open triangle*) and from Mackwell et al. (2005) (*dashed line*) for the same chemical composition and calculated for the Ni–NiO buffer are included

If charge neutrality were defined by Eq. 2 with $[\mathrm{Fe}^{\bullet}_{\mathrm{Me}}] = 2[\mathrm{V}''_{\mathrm{Me}}]$, we would expect an oxygen fugacity exponent of 1/6, an x exponent of $B = 2/3$ and a water fugacity exponent of 1/2. Using this oxygen fugacity exponent and the energy for the Ni–NiO reaction from O'Neill and Wall (1987), the contribution of the buffer reaction to the activation energy would be around 80 kJ mol^{-1}, resulting in an activation energy for interdiffusion of ~193 kJ mol^{-1}, which is very close to the activation energy measured for the anhydrous interdiffusion of iron and magnesium in (Mg,Fe)O of 209 kJ mol^{-1} (Mackwell et al. 2005). In this case, the enhanced diffusion in the presence of hydrogen would result simply from the increase in total vacancy concentration due to incorporation of hydrogen-vacancy defect associates $\{2(\mathrm{OH})^{\bullet}_{\mathrm{O}} - \mathrm{V}''_{\mathrm{Me}}\}^{\times}$. Although the concentration of these uncharged hydrous defect associates increases linearly with water fugacity, which is consistent with the water solubility law (Kohlstedt et al. 1996; Bolfan-Casanova et al. 2002), it does not vary with increasing iron content. Thus, it is inconsistent with the observation of $B \approx 0.8$ from the experiments.

If charge neutrality were defined by Eq. 6 with $[(OH)_O^{\bullet}] = 2[V''_{Me}]$, we would expect oxygen fugacity and x exponents of 0, and a water fugacity exponent of 1/3 for $[V''_{Me}]$. The observation of a strong dependence of interdiffusion on x (Fig. 4) is inconsistent with this charge neutrality condition.

If charge neutrality were defined by Eq. 10 with $[(Fe)_{Me}^{\bullet}] = [\{(OH)_O^{\bullet} - V''_{Me}\}']$, we would expect an oxygen fugacity exponent of 1/8, an x exponent of $B = 1/2$, and a water fugacity exponent of 1/3. While this value of B is smaller than the observed value of $B \approx 0.8$, this charge neutrality condition is the most consistent with the observations. Using an oxygen fugacity exponent of 1/8 and the energy for the Ni–NiO reaction from O'Neill and Wall (1987), the activation energy for interdiffusion would be ~215 kJ mol^{-1}.

Transition in charge neutrality condition

Under anhydrous or hydrous conditions, a transition from one charge neutrality to another may occur as function of $x \approx [Fe_{Me}^{\times}]$ (see Sect. 4). From point defect theory and as noted above, we would expect an x exponent of $B = 2/3$ or 1/2, depending on which charge neutrality condition is appropriate. However, the global fit to Eq. 19 yields $B = 0.8 \pm 0.1$. In order to avoid the section of the concentration profile where other charge neutrality conditions might control the point defect behavior and affect the Fe–Mg interdiffusion, a second global fit to the data was performed for a more limited range of iron content with $0.05 < x < 0.2$. In this case, the value of B obtained from the fit decreases to a value of 0.7 ± 0.1 with a parallel decrease of the C parameter from –80 to –90 kJ mol^{-1}. In both global fits, the measured value of Q is the same ~270 kJ mol^{-1} and the value of D_0 is ~5 ± 1. Thus, although a change in charge neutrality may occur at iron contents below $x = 0.05$, the associated change in diffusivity is below the resolution of the present data set.

Implication for the rheological properties of the lower mantle

The rheological properties of solids in the diffusion creep domain are essentially controlled by the self-diffusivity of the slowest ionic species diffusion along the fastest path, through the grain interiors or along the grain boundaries. For the periclase containing iron under lower mantle conditions, it has been argued that Fe and Mg ions might be the slowest diffusing species (Yamazaki and Karato 2001) with oxygen moving faster along grain boundaries. In this case, Fe and Mg diffusion through grain interiors would control the rheological properties of periclase. However, the increase in cationic diffusivity due to the presence of hydrogen observed in the present study (as well as by Chakraborty and Costa 2004; Hier-Majumber et al. 2004) is also expected to enhance the anion diffusivity in periclase, as well as in perovskites.

Although (Mg,Fe)O represents only ~15% of the volume of the Earth's lower mantle, the strength of this phase is expected to have important effects on the rheological properties of this region. It is estimated that (Mg,Fe)O is considerably weaker than silicate perovskite with a viscosity contrast of ~3 orders of magnitude (e.g., see Yamazaki and Karato 2001), but (Mg,Fe)O is unlikely to exert a major effect on rheology since it does not generally form an interconnected (network) solid phase (Handy 1994). However, some minor weakening may be anticipated, as the presence of a distributed, weaker phase may result in a relaxation of the von Mises criterion for homogeneous flow (von Mises 1928; Paterson 1969), allowing the perovskite to flow with fewer dislocation slip systems (e.g., Hirth and Kohlstedt 1996).

Deformation to high strain, as occurs within shear zones, can promote separation of phases. Recently, phase segregation has been experimentally reproduced for various systems, including olivine + chromite + MORB, (Holtzman et al. 2003), calcite + anhydrite (Barnhoorn et al. 2005), and anorthite + nickel (Larkin et al. 2005) as well as replicated by theoretical studies (Holtzman et al. 2005; Katz et al. 2006). By analogy, bands of (Mg,Fe)O might form an interconnected network and act as weak structures in the lower mantle that promote strain localization. Deformation in these zones could occur either by dislocation or by diffusion creep. Enhanced diffusion of iron and magnesium due to the presence of hydrogen might be expected to result in a modest decrease in strength for deformation by dislocation creep processes, while a larger effect on mechanical behavior might be anticipated if diffusion creep is the dominant mechanism of deformation in the lower mantle (e.g., Yamazaki and Karato 2001).

Acknowledgments SD thanks Christian Holzapfel for helpful advice at the early stage of the project, Mark Zimmerman for his generous assistance with running the Paterson apparatus, Nathalie Bolfan-Casanova for fervently and generously debating issues on point defects in (Mg,Fe)O, Catherine McCammon for Mössbauer analysis of the starting material, and Hans Keppler for access to his FTIR lab at the Bayerisches Geoinstitut. Electron microprobe analyses were carried out (with the help of Ellery Frahm) at the Electron Microprobe Laboratory, Department of Geology and Geophysics, University of Minnesota-Twin Cities. NSF supported the research through the grant NSF EAR-0337012 (to SJM) and NSF EAR-0439747 (to DLK). This paper is LPI publication #1326.

References

Bahr K, Simpson F (2002) Electrical anisotropy below low- and fast- plates: palaeoflow in the upper mantle? Science 295:1270–1272

Barnhoorn A, Bystricky M, Kunze K, Burlini L, Burg J-P (2005) Strain localisation in bimineralic rocks: experimental deformation of synthetic calcite-anhydrite aggregates. Earth Planet Sci Lett 240:748–763

Bell D, Rossman G, Maldener J, Endisch D, Rauch F (2003) Hydroxide in olivine: a quantitative determination of the absolute amount and calibration of the IR spectrum. J Geophys Res 108(B2). doi:10.1029/2001JB000679

Bolfan-Casanova N (2000) The distribution of water in the Earth's mantle: an experimental and infrared study. PhD Thesis, Universität Bayreuth

Bolfan-Casanova N (2005) Water in the Earth's mantle. Mineral Mag 69:229–257

Bolfan-Casanova N, Mackwell S, Keppler H, McCammon C, Rubie DC (2002) Pressure dependence of H solubility in magnesiowüstite up to 25 GPa: implications for the storage of water in the Earth's lower mantle. Geophys Res Lett 29:89/81–89/84

Chakraborty S, Costa F (2004) Fast diffusion of Si and O in San Carlos olivine under hydrous conditions. Geochim Cosmochim Acta 68:A275

Chopra PN, Paterson MS (1984) The role of water in the deformation of dunite. J Geophys Res 89:7861–7876

Demouchy S, Mackwell SJ (2003) Water diffusion in synthetic iron-free forsterite. Phys Chem Miner 30:486–494

Fiquet G, Andrault D, Dewaele A, Charpin T, Kunz M, Haüsermann D (1998) P–V–T equation of state of $MgSiO_3$. Phys Earth Planet Int 105:21–31

Gonzalez R, Chen Y, Tsang KL (1982) Diffusion of deuterium and hydrogen in doped and undoped MgO. Phys Rev B 26:4637–4645

Gordon RS (1985) Diffusional creep phenomena in polycrystalline oxides. In: Schock RN (ed) Point defect in minerals. Geophysical Monograph, vol 31. American Geophysical Union, Washington, DC, pp 132–140

Gourdin WH, Kingery WD (1979) The defect structure of MgO containing trivalent cation solutes: shell mode calculations. J Mat Sci 14:2053–2073

Guyot F, Madon M, Peyronneau J, Poirier JP (1988) X-ray microanalysis of high-pressure/high-temperature phases synthesized from natural olivine in a diamond anvil cell. Earth Planet Sci Lett 90:52–64

Handy MR (1994) flow laws for rocks containing two non-linear viscous phases: a phenomenological approach. J Struct Geol 16:287–301

Hier-Majumber S, Anderson IM, Kohlstedt DL (2004) Influence of protons on Fe–Mg interdiffusion in olivine. J Geophys Res 110. doi:10.1029/2004JB003292

Hirth G, Kohlstedt DL (1996) Water in the oceanic upper mantle: implications for rheology, melt extraction and the evolution of the lithosphere. Earth Planet Sci Lett 144:93–108

Holtzman BK, Groebner NJ, Zimmerman ME, Ginsberg SB, Kohlstedt D (2003) Stress-driven melt segregation in partially molten rocks. Geochem Geophys Geosys 4(5). doi:10.1029/2001GC000258

Holtzman BK, Kohlstedt DL, Phipps Morgan J (2005) Viscous energy dissipation and strain partitionning in partially molten rocks. J Petrol. doi:10.1029/petrology/egi1065

Holzapfel C (2004) Fe–Mg interdiffusion at high pressures in mineral phases relevant for the Earth's mantle. PhD Thesis, Universität Bayreuth

Holzapfel C, Rubie DC, Mackwell SJ, Frost DJ (2003) Effect of pressure on Fe–Mg interdiffusion in $(Fe_xMg_{1-x})O$, ferropericlase. Phys Earth Planet Inter 139:21–34

Huang X, Xu Y, Karato S-I (2005) Water content in the transition zone from electrical conductivity of wadsleyite and ringwoodite. Nature 434:746–749

Ingrin J, Skogby H (2000) Hydrogen in nominally anhydrous upper-mantle minerals: concentration levels and implications. Eur J Mineral 12:543–570

Ito E, Takahashi E (1987) Melting of peridotite at uppermost lower-mantle conditions. Nature 328:514–517

Jacobsen SD, Smyth JR, Spetzler HA, Frost DJ (2004) Sound velocities and elastic constant of iron-bearing hydrous ringwoodite. Phys Earth Planet Inter 143–144:47–56

Karato S-I (1990) The role of hydrogen diffusivity in the electrical conductivity of the upper mantle. Nature 347:272–273

Katz RF, Speigelman M, Holtzman B (2006) The dynamics of melt and shear localization in partially molten aggregates. Nature 442:676–678

Kohlstedt DL, Mackwell SJ (1998) Diffusion of hydrogen and intrinsic point defects in olivine. Z Phys Chem 207:147–162

Kohlstedt DL, Keppler H, Rubie DC (1996) Solubility of water in the α, β and γ phases of $(Mg,Fe)_2SiO_4$. Contrib Mineral Petrol 123:345–357

Kröger FA, Vink HJ (1956) Relation between the concentrations of imperfections in crystalline solids. Academy Press, New York

Larkin L, Zimmerman ME, Kohlstedt DL (2005) Phase separation during deformation of a two-phase rock. Eos Trans AGU 86 Fall Meet Suppl Abs T41C-1320

Libowitzky E, Rossman G (1996) Principles of quantitative absorbance measurements in anisotropc crystals. Phys Chem Mineral 23:319–327

Mackwell SJ, Bystricky M, Sproni C (2005) Fe–Mg interdiffusion in (Mg,Fe)O. Phys Chem Mineral. doi:10.1007/s00269-005-0013-6

Mackwell SJ, Kohlstedt DL, Paterson MS (1985) The role of water in the deformation of olivine single crystals. J Geophys Res 90:11319–11333

Matano C (1933) On the relation between diffusion coefficients and concentrations in solids metals (the nickel–copper system). Jpn J Phys 8:109–113

Mei S, Kohlstedt DL (2000) Influence of water on the plastic deformation of olivine aggregates: 2. Diffusion creep regime. J Geophys Res 105:21,471–421,481

Nakamura A, Schmalzried H (1984) On the Fe^{2+}–Mg^{2+}-interdiffusion in olivine (II). Ber Bunsenges Phys Chem 88:140–145

O'Neill HS, Wall V (1987) The olivine-orthopyroxene-spinel oxygen geobarometer, the nickel precipitation curve, and the oxygen fugacity of Earth's upper mantle. J Petrol 28:1169–1191

Paterson M (1969) The ductile of rocks. In: Argon AS (ed) Physics of strength and plasticity. MIT Press, Cambridge, pp 377–392

Paterson M (1982) The determination of hydroxyl by infrared absorption in quartz, silicate glasses and similar materials. Bull Minéral 105:20–29

Paterson MS (1990) Rock deformation experimentation. In: Duba A (ed) The brittle–ductile transition in rocks: the Head Volume, vol 56. Geophysical Monograph Serie American Geophysical Union, Washington DC, pp 187–194

Pitzer KS, Sterner SM (1994) Equations of state valid continuously from zero to extreme pressures for H_2O and CO_2. J Chem Phys 101:3111–3116

Rauch M, Keppler H (2002) Water solubility in orthopyroxene. Contrib Mineral Petrol 143:525–536

Ringwood AE (1991) Phase transitions and their bearing on the constitution and dynamics of the mantle. Geochim Cosmochim Acta 55:2083–2110

Schmalzried H (1981) Solid state reactions. Verlag Chemie, Weinheim, 254pp

Shinoda K, Yamakata M, Nanba T, Kimura H, Moriwaki T, Kondo Y, Kawamoto T, Niimi N, Miyoshi N, Aikawa N (2002) High-pressure phase transition and behavior of protons in brucite $Mg(OH)_2$: a high-pressure–temperature study using IR synchrotron radiation. Phys Chem Miner 29:396–402

Valet P-M, Plushkell W, Engell H-J (1975) Equilibria between MgO–FeO–Fe_2O_3 solid solutions and oxygen. Arch Eisenhuettenwes 46:383–388

Von Mises R (1928) Mechanik der plastichem Formänderung von Kristallen. Z Ang Math Mech 8:161–185

Wang Z, Hiraga T, Kohlstedt DL (2004) Effect of H+ on Fe–Mg interdiffusion in olivine, $(Fe–Mg)_2SiO_4$. Appl Phys Lett 85:209–211

Wang J, Mookherjee M, Xu Y, Karato S (2006) The effect of water on the electrical conductivity of olivine. Nature 443:977–980

Yamazaki A, Irifune T (2003) Fe–Mg interdiffusion in magnesiowustite up to 35 GPa. Earth Planet Sci Lett 216:301–311

Yamazaki D, Karato S-I (2001) Some mineral physics constraints on the rheology and geothermal structure of Earth's lower mantle. Am Mineral 86:385–381

Yoshino T, Matsuzaki T, Yamashita S, Katsura T (2006) Hydrous olivine unable to account for conductivity anomaly at the top of the asthenosphere. Nature 443:973–976

Zhao Y, Ginsberg S, Kohlstedt D (2004) Solubility of hydrogen in olivine: dependence on temperature and iron content. Contrib Mineral Petrol 147:155–161